

NASA TECHNICAL NOTE



NASA TN D-5171

C.1

NASA TN D-5171



LOAN COPY: RETURN TO
AFWL (WLIL-2)
KIRTLAND AFB, N MEX

ON THE DESIGN OF ACOUSTIC LINERS
FOR ROCKET ENGINES: HELMHOLTZ
RESONATORS EVALUATED WITH
A ROCKET COMBUSTOR

by Bert Phillips, Ned P. Hannum, and Louis M. Russell

Lewis Research Center

Cleveland, Ohio



ON THE DESIGN OF ACOUSTIC LINERS FOR ROCKET ENGINES:
HELMHOLTZ RESONATORS EVALUATED
WITH A ROCKET COMBUSTOR

By Bert Phillips, Ned P. Hannum, and Louis M. Russell

Lewis Research Center
Cleveland, Ohio

NATIONAL AERONAUTICS AND SPACE ADMINISTRATION

For sale by the Clearinghouse for Federal Scientific and Technical Information
Springfield, Virginia 22151 - CFSTI price \$3.00

ABSTRACT

A study was made to improve the design of rocket engine acoustic liners. Helmholtz resonators with variable cavity depths were tested with an unstable rocket combustor. Combustor pressure oscillations inside the resonators and in the combustor and the phase angles between them were measured. From these measurements resonator aperture effective lengths were calculated. A new correlation for the effective lengths at high mean gas velocities is presented. A nonlinear resonator model is evaluated and used to calculate the aperture resistance. The calculated resistances were correlated by an empirical function of the mean and oscillatory flows.

ON THE DESIGN OF ACOUSTIC LINERS FOR ROCKET ENGINES:
HELMHOLTZ RESONATORS EVALUATED
WITH A ROCKET COMBUSTOR

by Bert Phillips, Ned P. Hannum, and Louis M. Russell
Lewis Research Center

SUMMARY

A study was made to improve the design of acoustic liners for rocket engines. Helmholtz resonator aperture effective lengths were determined from rocket combustor measurements and a nonlinear resonator model was derived, evaluated, and used to calculate aperture resistance. To facilitate combustor measurements, five Helmholtz resonators with remotely variable cavity depths and known cavity gas properties were tested with a hydrogen-oxygen rocket engine. The engine was operated near the hydrogen temperature screech stability limit to produce measurable small pretransition oscillations. A measurement of the phase relation between the oscillatory pressure on both sides of the resonator aperture gave the tuned cavity depths for the resonators. Aperture effective lengths were calculated from the tuned cavity depths and were compared with the mean gas velocity through the aperture. A new correlation for the effective length correction at high mean gas velocities is presented.

The measured ratio of cavity to chamber oscillatory pressure was compared with the results of the theoretical nonlinear resonator model. The results compared favorably with experimental data, and the theoretical model was then used to calculate the resonators' resistance as a function of mean and oscillatory aperture flows. These theoretically calculated resistances were correlated by an empirical function of the mean and oscillatory flows.

INTRODUCTION

The use of acoustic damping to suppress rocket engine combustion instability has been extensively investigated and reported in the literature (refs. 1 and 2). The present

design of the acoustic dampers is based on maximizing the acoustic absorption of an array of Helmholtz resonators mounted on the walls of the combustion chamber. One method for calculating the damping has been reported in reference 1. This method depends on a knowledge of the correct values for resonator acoustic resistance θ and resonator aperture effective length l_{eff} in a rocket combustor. Both the θ and l_{eff} are functions of the cavity gas properties, the acoustic wave amplitude, the resonator geometry, and any mean gas flow, whether past or through the aperture. Up to the present time, the calculation of θ and l_{eff} has depended on estimating wave amplitudes, gas flows, and gas properties in the combustor and using these values in empirical correlations which are based on results with cold air flow (refs. 3 to 6).

Errors in estimating these values can lead to large errors in calculating the acoustic absorption. In an effort to eliminate some of the design errors, the objectives of the present experiment were (1) to determine the aperture effective length l_{eff} from phase measurements made in a resonator mounted in a rocket combustor and (2) to develop a nonlinear resonator model, similar to that presented in reference 7, verify the model with resonator pressure measurements, and use the model to calculate θ , the resistance.

To obtain the phase measurements, five Helmholtz resonators with variable cavity depths were mounted on a rocket combustor. The resonators were continuously purged with helium to assure known cavity gas properties. The combustor was operated near the hydrogen temperature screech stability limit to produce measurable combustor pressure oscillations. By measuring the phase relation between the oscillatory pressures on both sides of the resonator aperture as the cavity depths were varied, the cavity depths corresponding to tuning (oscillatory combustor pressure frequency = Helmholtz resonance frequency) were obtained. In the same manner as presented in reference 8, the l_{eff} was obtained from the known values of tuned cavity depth, oscillatory combustor pressure frequency, resonator geometry, and cavity gas sonic velocity.

The nonlinear resonator model is that presented in reference 7, modified for the presence of the helium purge flow. The model was used to calculate values of cavity pressure oscillation amplitudes corresponding to a range of values of combustor pressure oscillation amplitudes. To verify the model, values of cavity and combustor pressure oscillation amplitudes were measured and compared with the calculated values. The model was then used to calculate values of the ratio of combustor pressure oscillation amplitude to the component of the aperture velocity which is in phase with the pressure. The normalized value of the ratio is θ , the aperture resistance.

The investigation reported herein was conducted at the Rocket Engine Test Facility of Lewis Research Center using a liquid hydrogen-liquid oxygen rocket combustor. The combustor had an inside diameter of 10.78 inches (27.2 cm) and was operated at the nominal values of 300-psia (2.07×10^6 -N/m² abs) chamber pressure, 12 500-pound (55 600-N) sea-level thrust, and 95 percent C^* combustion efficiency.

SYMBOLS

A	aperture area, ft ² (m ²)
C	adiabatic constant
C*	characteristic exhaust velocity, ft/sec (m/sec)
c	gas sonic velocity, ft/sec (m/sec)
c _p	heat capacity, ft/ ⁰ R (m/K)
d	aperture diameter, ft (m)
f	frequency, Hz
g _c	gravitational constant
l	aperture length, ft (m)
l _{eff}	aperture effective length, ft (m)
M	average mass per cross-sectional area, kg/ft ² (kg/m ²)
\mathcal{M}	molecular weight, kg/kg-mole
P	total pressure, psf (N/m ²)
p	static pressure, psf (N/m ²)
R	nonnormalized resistance, kg/(ft ²)(sec); kg/(m ²)(sec)
r	dimensionless weight flow
T	total temperature, ⁰ R (K)
U	aperture velocity, ft/sec (m/sec)
ΔU	mean-to-peak velocity in aperture, ft/sec (m/sec)
\bar{U}	mean velocity in aperture, ft/sec (m/sec)
$\bar{\bar{U}}$	mean velocity past aperture, ft/sec (m/sec)
V	cavity volume, ft ³ (m ³)
W	defined by eq. (11)
w	purge weight flow, lb/sec (kg/sec)
α	normal acoustic absorption coefficient
$\bar{\alpha}^2$	$(C_{II}/C_I)^{1/\gamma}$
β	dimensionless cavity geometry
γ	ratio of heat capacities

δ	aperture effective length correction, ft (m)
θ	acoustic resistance of resonator
ρ	gas density lb/ft ³ (kg/m ³)
σ	array open area ratio
τ	time, sec
Φ	acoustic resistance of resonator array
ω	angular frequency, 1/sec
ω_0	resonant frequency, 1/sec

Subscripts:

av	average
cavity	resonator cavity
max	maximum
o	reference condition
I	chamber side
II	cavity side
1	chamber side of aperture
2	cavity side of aperture
+	velocity into cavity
-	velocity out of cavity

Superscript:

'	nondimensional
---	----------------

APPARATUS

Injector

A 421-element flat-faced concentric-tube injector was used for the tests; the hydrogen-oxygen injection area ratio was 5.18. The injector faceplate was copper with a hexagonal element pattern covering 85 percent of the face. A faceplate view of the injector is shown in figure 1.

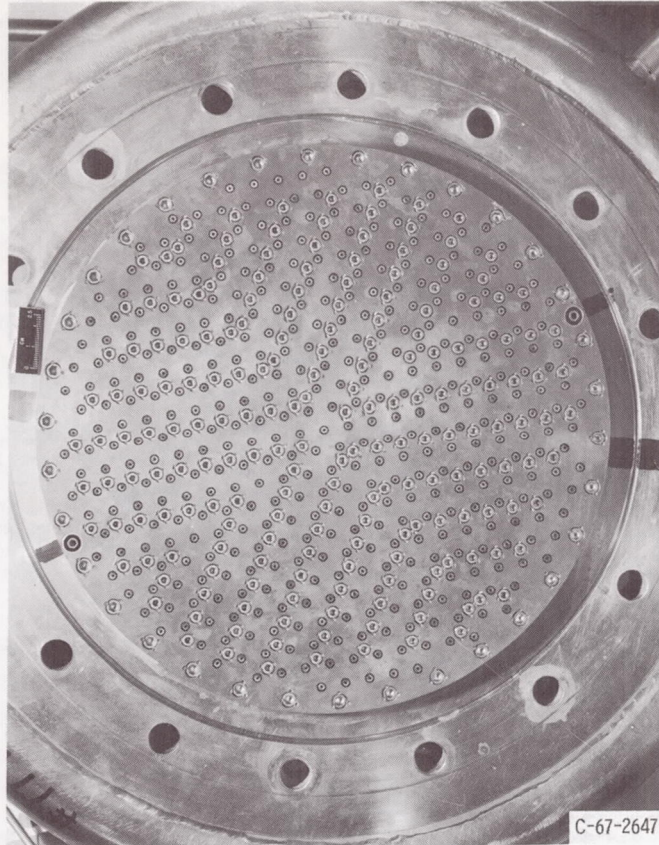


Figure 1. - Injector face.

Engine

The heat-sink engine used had an inside diameter of 10.78 inches (27.2 cm) with a cylindrical section 10 inches (25.4 cm) long and a converging section 4 inches (10.16 cm) long. The contraction ratio was 3.00. The engine was operated at a nominal mixture ratio of 5 and a chamber pressure of 300 psia (2.07×10^6 N/m² abs).

Resonators

Five resonators in a single axial row were tested simultaneously. The resonators were equipped with hydraulically actuated pistons for simultaneously varying the cavity depths during a run. The cavity depth was varied from $\frac{1}{2}$ to $2\frac{1}{2}$ inches (1.27 to 6.35 cm) in 2 seconds. The aperture thickness was $\frac{3}{16}$ inch (0.476 cm); the aperture diameter was $\frac{1}{4}$ inch (0.64 cm); and the piston diameter was $\frac{7}{8}$ inch (2.22 cm). In addition to the instrumentation discussed in the next section, each resonator was equipped with a

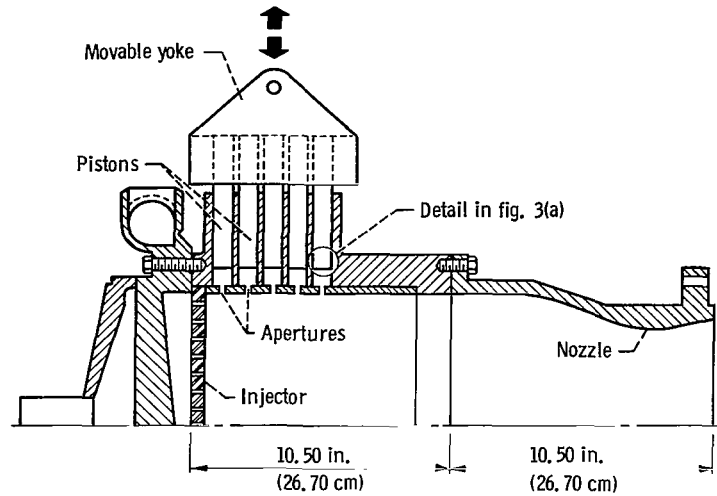


Figure 2. - Injector resonator nozzle assembly.

helium gas bleed line. A sketch of the resonators is shown in figures 2 and 3(a), and a photograph of the piston assembly is shown in figure 3(b).

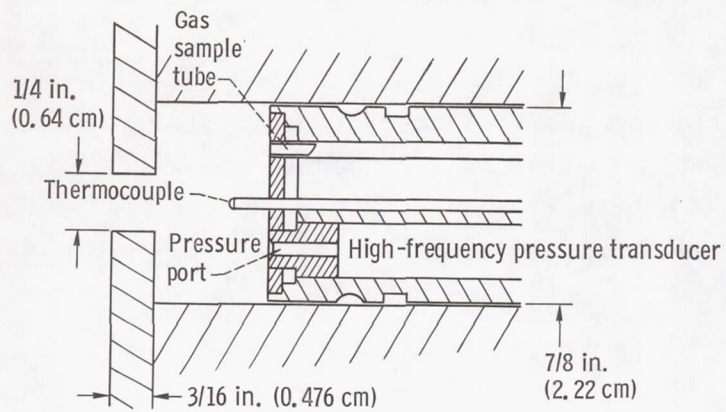
Facility

The Rocket Engine Test Facility of the Lewis Research Center is a 50 000-pound- (224 000-N-) thrust sea-level test stand equipped with an exhaust gas scrubber and muffler. The facility utilizes a pressurized propellant system to deliver the propellants to the engine from the storage tanks. The facility is operated remotely from a control room located 2000 feet (610 m) away. A more complete description is given in reference 1.

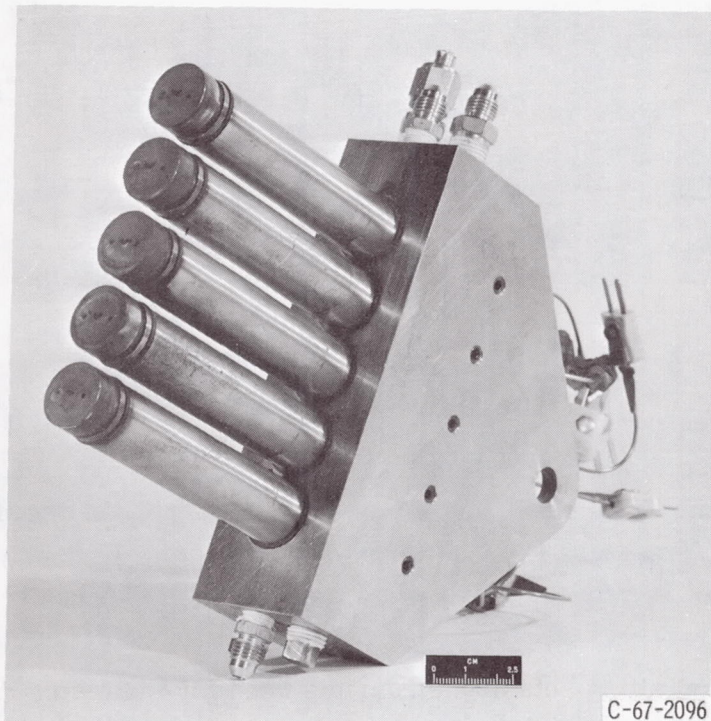
Instrumentation

There were two distinct sets of instruments used for the tests, those for monitoring engine operation and those associated with the resonators. The instruments for engine operation are the same as those discussed in reference 1.

The resonator instrumentation included a Chromel-Alumel open ball thermocouple within the cavity for measuring cavity gas temperature. In addition, a 1/16-inch (0.159-cm) inside-diameter line was connected to a gas bottle to sample the cavity gas. Two high-frequency pressure transducers were used with each resonator cavity. One was mounted in the cavity piston, as shown in figure 3(b), and the other was mounted on the inside of the combustion chamber and $2\frac{1}{2}$ inches (6.35 cm) circumferentially from the



(a) Cavity piston.



(b) Hydraulic ram with cavity pistons. Each piston contains a high-frequency transducer, a thermocouple, and a gas bleed line.

Figure 3. - Detail of cavity piston and hydraulic ram.

aperture (the closest it could be placed). In addition, a high-frequency transducer was mounted on the inside of the chamber at an axial position corresponding to a resonator but displaced 135° . This was done to determine whether a resonant chamber mode was standing or spinning. The high-frequency transducers had nominal resonant frequencies of 10 000 hertz and a frequency response that was flat to 6000 hertz as mounted. The output from the high-frequency channels was recorded on analog tape and was later analyzed using a series of band pass filters and a phase meter to determine the amplitude frequency distribution of both the cavity and combustion pressure oscillations as well as the phase relation between them.

THEORY

The theory section is divided into two parts; in the first part, l_{eff} or aperture effective length is calculated, and in the second, the nonlinear resonator model is derived.

Determination of l_{eff}

The Helmholtz resonance frequency of a cavity-orifice combination is the following (ref. 1):

$$\omega_0 = c_{\text{cavity}} \sqrt{\frac{A}{l_{\text{eff}} V}} \quad (1)$$

As shown in reference 8, when the Helmholtz resonant frequency is equal to the impressed wave frequency, the phase angle between the impressed oscillatory pressure and the cavity oscillatory pressure is 90° . If the cavity volume V is altered so as to vary ω_0 until the phase angle between cavity and impressed wave pressure is 90° , then the impressed wave frequency ω equals ω_0 . Since ω is known from spectral analysis of the combustor pressure oscillations, c_{cavity} is defined by gas purging, and A is fixed, then, at the value of V corresponding to $\omega = \omega_0$, l_{eff} is defined.

Nonlinear Resonator Model

As an aid in formulating the model, a sketch of a single resonator with relevant

$$\frac{dU}{d\tau} = \frac{P_1 - P_2}{\frac{l_{\text{eff}}}{2g_c} \left[\left(\frac{P_1}{C_I} \right)^{1/\gamma} + \left(\frac{P_2}{C_{II}} \right)^{1/\gamma} \right]} \quad (6)$$

Mass conservation for the cavity is satisfied by

$$V \frac{d\rho_{II}}{d\tau} = \dot{w} + \rho_2 A U \quad (7)$$

where \dot{w} is the helium purge weight flow and U is considered positive when directed into the cavity. The addition of the \dot{w} then is the only modification to the model presented in reference 7.

Substituting equation (5) into equation (7) yields

$$V \frac{d \left(\frac{\rho_{II}}{C_{II}} \right)^{1/\gamma}}{d\tau} = \dot{w} + \left(\frac{P_2}{C} \right)^{1/\gamma} A U \quad (8)$$

When U is positive with flow into the cavity, the C of equation (8) is C_I ; whereas for U_- , $C = C_{II}$.

The loss in the resonator is ascribed to loss of velocity head of the exiting jet. Therefore, for U_+ , the following hold:

$$P_1 = P_I \left(1 - W_+^2 \right)^{\gamma/(\gamma-1)} \quad (9)$$

$$P_2 = P_{II} \quad (10)$$

where W_+ is defined by

$$W_+ = \frac{U_+}{\sqrt{2c_p g_c T_I}} \quad (11)$$

For U_- , the following is assumed:

$$P_1 = P_I \quad (12)$$

$$p_2 = P_{II} (1 - W_-^2)^{\gamma/(\gamma-1)} \quad (13)$$

where W_- is defined by

$$W_- = \frac{U_-}{\sqrt{2c_p g_c T_{II}}} \quad (14)$$

Substituting equations (9) to (14) into equations (6) and (8) results in the following, for U_+ :

$$\frac{dU_+}{d\tau} = \frac{P_I (1 - W_+^2)^{\gamma/(\gamma-1)}}{\frac{l_{eff}}{2g_c} \left\{ \left[P_I (1 - W_+^2)^{\gamma/(\gamma-1)} \right]^{1/\gamma} + \left(\frac{P_{II}}{C_I} \right)^{1/\gamma} \right\}} \quad (15)$$

$$\frac{dP_{II}}{d\tau} = \frac{\gamma \dot{w}}{V} \frac{C_{II}^{1/\gamma}}{P_{II}^{(1/\gamma)-1}} + \frac{\gamma AU_+}{V} \left(\frac{C_{II}}{C_I} \right)^{1/\gamma} P_{II} \quad (16)$$

$$W_+ = \frac{U_+}{\left(\frac{2\gamma}{\gamma-1} \right)^{1/2} (P_I)^{(\gamma-1)/2\gamma} C_I^{1/2\gamma}} \quad (17)$$

and, for U_- :

$$\frac{dU_-}{d\tau} = \frac{P_I - P_{II} (1 - W_-^2)^{\gamma/(\gamma-1)}}{\frac{l_{eff}}{2g_c} \left\{ \left(\frac{P_I}{C_{II}} \right)^{1/\gamma} + \left[\frac{P_{II} (1 - W_-^2)^{\gamma/(\gamma-1)}}{C_{II}} \right]^{1/\gamma} \right\}} \quad (18)$$

$$\frac{dP_{II}}{d\tau} = \frac{\gamma \dot{w}}{V} \frac{C_{II}^{1/\gamma}}{P_{II}^{(1/\gamma)-1}} + \frac{\gamma A U_-}{V} P_{II} (1 - W_-^2)^{\gamma/(\gamma-1)} \quad (19)$$

$$W_- = \frac{U_-}{\left(\frac{2\gamma}{\gamma-1}\right)^{1/2} (P_{II})^{(\gamma-1)/2\gamma} C_{II}^{1/2\gamma}} \quad (20)$$

To normalize these equations, the following parameters are chosen:

$$\left. \begin{aligned} \tau' &= \frac{\tau c_0}{l_{\text{eff}}} & \beta &= \frac{A l_{\text{eff}}}{V} & \bar{\alpha}^2 &= \left(\frac{C_{II}}{C_I}\right)^{1/\gamma} \\ P'_1 &= \frac{P_I}{P_0} & P'_2 &= \frac{P_{II}}{P_0} & U' &= \frac{U}{c_0} & r &= \frac{\dot{w}}{\rho_0 c_0} \end{aligned} \right\} \quad (21)$$

Substituting the preceding parameters into equations (15) to (20) gives,

for U'_+ :

$$\frac{dU'_+}{d\tau'} = \frac{2}{\gamma} \frac{P'_1 (1 - W_+^2)^{\gamma/(\gamma-1)} - P'_2}{\left[P'_1 (1 - W_+^2)^{\gamma/(\gamma-1)} \right]^{1/\gamma} + (P'_2)^{1/\gamma}} \quad (22)$$

$$\frac{dP'_2}{d\tau'} = \gamma \beta (P'_2)^{1-(1/\gamma)} r \bar{\alpha}^2 + \gamma \bar{\alpha}^2 \beta U'_+ \quad (23)$$

$$W_+ = \frac{U'_+}{\left(\frac{2}{\gamma-1}\right)^{1/\gamma} (P'_1)^{(\gamma-1)/2\gamma}} \quad (24)$$

for U'_- :

$$\frac{dU'_-}{d\tau'} = \frac{2\bar{\alpha}^2}{\gamma} \frac{P'_1 - P'_2(1 - W_-^2)^{\gamma/(\gamma-1)}}{(P'_1)^{1/\gamma} + \left[P'_2(1 - W_-^2)^{\gamma/(\gamma-1)} \right]^{1/\gamma}} \quad (25)$$

$$\frac{dP'_2}{d\tau'} = \gamma\beta r \bar{\alpha}^2 (P'_2)^{(\gamma-1)/\gamma} + \gamma\beta U'_- P'_2 (1 - W_-^2)^{1/(\gamma-1)} \quad (26)$$

$$W_- = \frac{U'_-}{\bar{\alpha}^2 \left(\frac{2}{\gamma-1} \right)^{1/2} (P'_2)^{(\gamma-1)/2\gamma}} \quad (27)$$

As discussed in reference 7, a reasonable approximation for $\bar{\alpha}^2$ is the following:

$$\bar{\alpha}^2 = \left(\frac{C_{II}}{C_I} \right)^{1/2} \sim \frac{\mathcal{M}_O T_{II}}{\mathcal{M}_{II} T_O} \quad (28)$$

Equations (22) to (27) were solved by a fourth-order Runge-Kutta method on a digital computer. The input pressure P'_1 was sinusoidal only. The normalized part of impedance of the resonator was obtained by dividing the maximum input pressure by the in-phase maximum oscillation U' so that the following equation resulted:

$$\theta = \frac{\Delta P_1}{\gamma \Delta U} \Big|_{\text{in phase}} \quad (29)$$

PROCEDURE

The resonators were tested in a rocket engine that was operating stably but near the instability boundary. In reference 1, it was shown that a hydrogen-oxygen rocket engine can be driven into full-scale instability or screech by sufficiently lowering the hydrogen inlet temperature. As the unstable transition temperature was approached from the stable regime, a low amplitude chamber pressure oscillation was found to be present

which remained until the abrupt screech transition point (ref. 9). It was under this pre-transition condition that the resonators were tested.

The first step in the testing sequence was to evaluate the screech transition temperature of the injector. The procedure for testing the resonator was to set an inlet hydrogen temperature about 15° R (9 K) above the stability transition temperature. The damping due to the five resonators was not sufficient to affect the stability limits. The helium gas bleed system was in operation at all times to fix the cavity gas composition. During engine startup, the helium purge was maintained at a high value to prevent the ignition spike from forcing hot combustion gases into the cavity. After steady-state combustion had been achieved, at some predetermined time in the run, the gas purge flow was reduced to the desired level and the five hydraulically operated pistons were moved simultaneously to increase the cavity volumes. During the piston motion, a valve in the gas sample system was opened and closed for a predetermined time and the gas sample storage bottles were filled to 300-psia (2.07×10^6 N/m² abs) chamber pressure. The total run time was $2\frac{1}{2}$ seconds.

RESULTS AND DISCUSSION

To determine the values of aperture effective length l_{eff} , it was necessary to measure the cavity and chamber oscillatory pressures, the phase relation between them, the cavity gas temperature, the cavity purge flow, and the cavity depth as a function of time for each run.

Typical results for a run are shown in figure 5. The cavity depth was maintained constant as the mean chamber pressure rose to a steady-state value of 300 psi (2.07×10^6 N/m²). At $\tau = 0.6$ second, the hydraulically controlled pistons were withdrawn and the cavity depth was linearly increased. The corresponding cavity gas temperature also changed during this period as shown in figure 5(b). In the initial portion of the run, a high purge flow was maintained to prevent the ignition spike from forcing hot gases into the cavity. From $\tau = 0.2$ to 0.6 second, the high purge pressure was gradually reduced to a value which was kept constant for the remainder of the run. The surge in temperature corresponded to the decrease in purge flow. At the screech transition point, the temperature of the cavity increased markedly. An example of the output of two high-frequency transducers (one in the resonator cavity, the other on the chamber wall), is shown in figure 5(c). For this particular run, it was not possible to maintain the hydrogen injection temperature above the transition temperature and high amplitude instability resulted at $\tau = 1.8$ seconds.

The phase relation between the two transducers is shown in figure 5(d). As the cavity depth was increased, the ratio of oscillatory chamber pressure frequency f_{wave} (5300 Hz) to cavity or Helmholtz resonant frequency was also increased and the phase re-

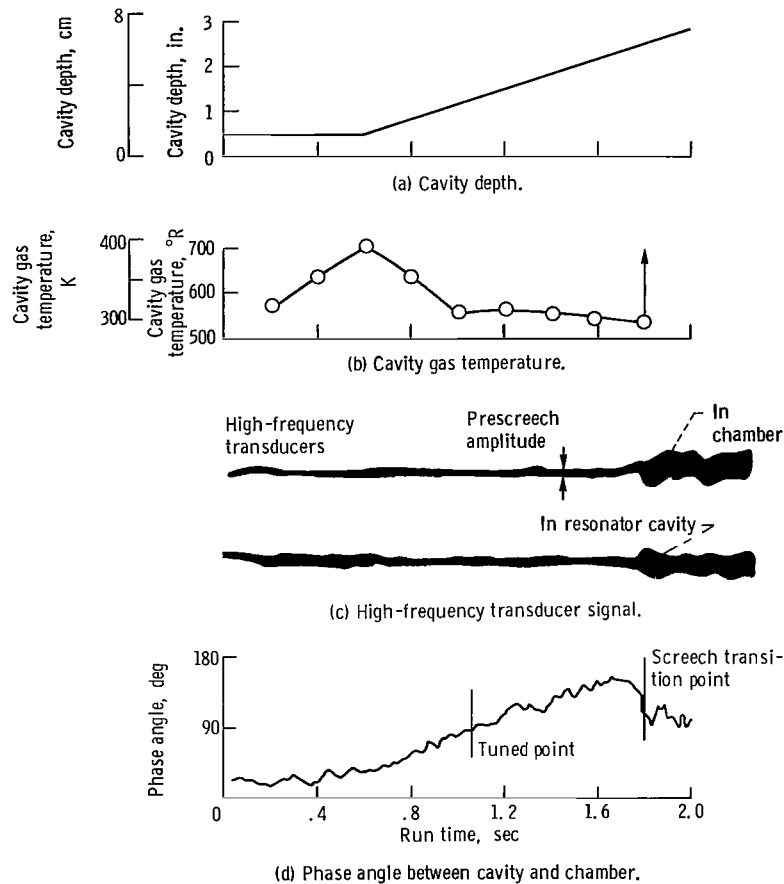


Figure 5. - Typical results for a run.

lation between the pressure oscillations changed as shown. Comparison of the outputs from the two transducers located 135° apart at the same axial position indicated that the chamber oscillation pattern or mode was standing rather than spinning. Thus, the phase angle between transducers located $2\frac{1}{2}$ inches (5.35 cm) from the aperture and inside the cavity corresponded to the phase relation across the aperture with no error due to the $2\frac{1}{2}$ -inch (5.35-cm) displacement introduced. At a phase lag of 90° , cavity reactance became zero and the wave frequency was equal to the cavity resonant frequency. This is the tuned condition.

An important step in analyzing the data was to obtain spectral analyses of the output of the high-frequency transducers as a function of cavity depth since this gives the value of f_{wave} or ω . A typical spectral analysis of the output of a high-frequency transducer mounted on the combustion chamber is presented in figure 6. The pretransition period is characterized by a frequency of 5300 hertz. After the screech transition, the amplitude increased markedly and the frequency shifted to 5700 hertz, corresponding to the second tangential mode.

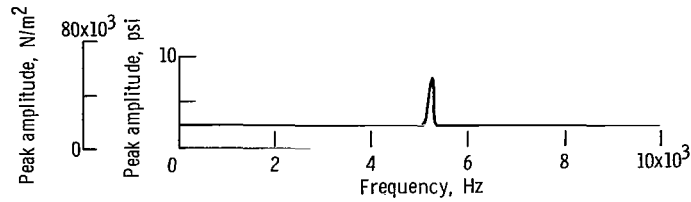


Figure 6. - Spectral analysis of signal from chamber high-frequency transducer for pretransition operation.

Calculation of Aperture Effective Length

The aperture effective lengths of the resonators were calculated in the same manner as described in the section Determination of λ_{eff} . Gas properties and the mean aperture velocities were defined by the helium purge, and the aperture area was fixed so that the cavity volume and aperture effective length controlled the resonant frequency. As the cavity volume or depth was increased, the phase angle between the pressure oscillations increased, as shown in figure 5. At a phase angle of 90° , corresponding to a 1/4-cycle lag, f_{wave} was equal to the $f_{\text{Helmholtz}}$ (ref. 8). Since f_{wave} was known (5300 Hz) and cavity volume V was known as a function of time, the aperture effective length could be calculated.

Before presenting the results of the λ_{eff} calculation, a brief discussion of the effects of mean flow through and past the aperture is in order. The effect of mean flow past an aperture on effective length was reported in reference 5 and is presented in figure 7. A mean flow of 394 feet per second (120 m/sec) reduces the aperture mass or ef-

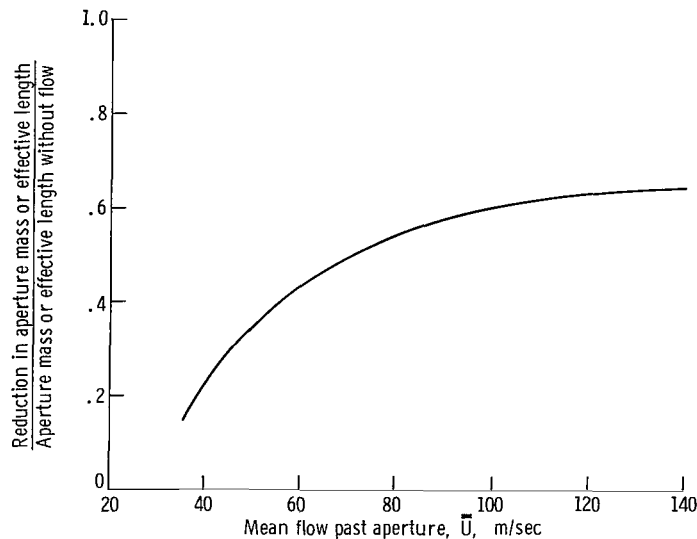


Figure 7. - Effect of mean flow past on aperture mass or λ_{eff} . Aperture length $l = 0.3$ centimeter; aperture diameter $d = 0.8$ centimeter. (See fig. 5 in ref. 5.)

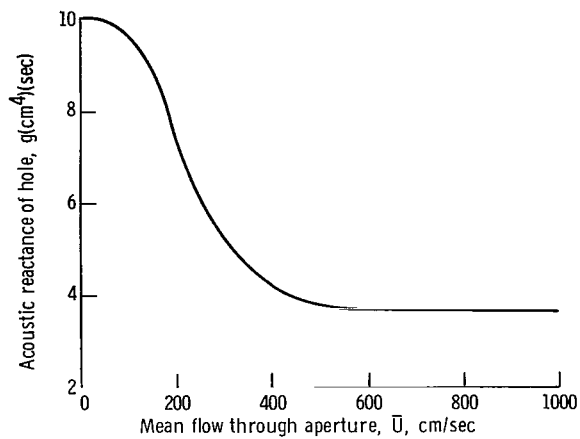


Figure 8. - Effect of aperture flow through on aperture reactance. Aperture length $l = 0.0508$ centimeter; aperture diameter $d = 0.357$ centimeter. (See fig. 13 in ref. 6.)

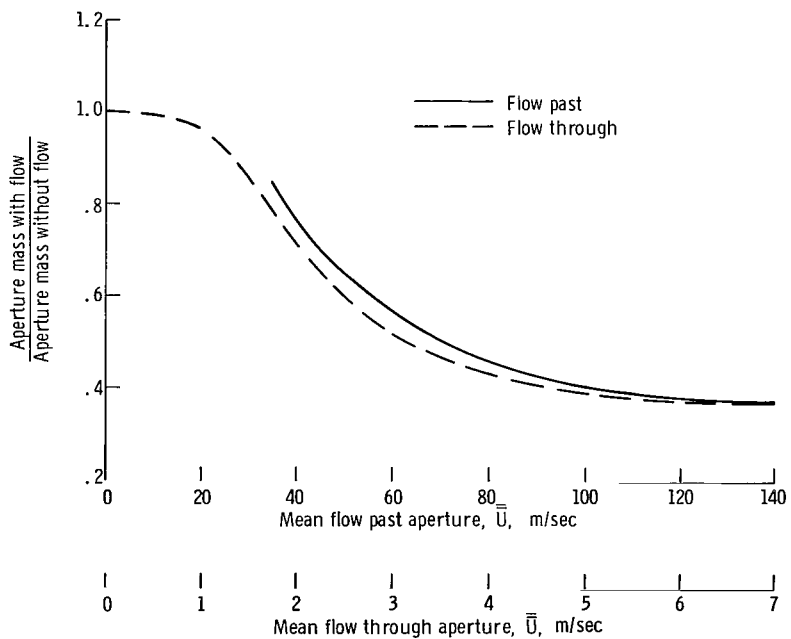


Figure 9. - Comparing effects of mean flow past and mean flow through on aperture mass.

fective length by a factor of 0.625 or reduces it to a minimum or saturated value of 0.375 times its nonflow value. A separate study, reported in reference 6, indicated that mean flow through the aperture would also have a strong effect on l_{eff} . The flow-through effect is presented in figure 8. Changes in acoustic reactance for this experiment are equivalent to changes in effective length. The results indicate a similar reduction with the flow through to that with flow past. In order to compare the two effects, both results are plotted as the ratio of l_{eff} with flow to l_{eff} without flow and are shown in figure 9. The agreement between the two effects indicate a similarity in l_{eff} reduction. Comparison of the flow velocities required for the same effect indicates the flow through is approximately 20 times as important as flow past. In the rocket engine environment discussed in this report, the mean flow past was approximately 1000 feet per second (305 m/sec) and the mean purge flow through the aperture was approximately 250 feet per second (76 m/sec). Either effect, or a combination of the two, was sufficient to reduce the aperture effective lengths to their minimum or saturated values. Therefore, the results presented in figure 10 are l_{eff} values which are saturated and thus independent of flow.

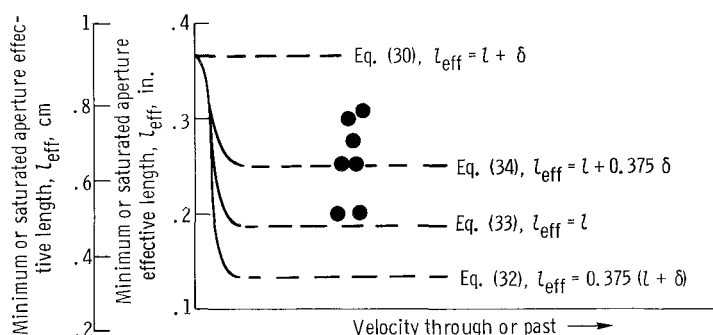


Figure 10. - Aperture effective length at large flow-past and flow-through velocities. Velocity past, 1000 feet per second (305 m/sec); velocity through, 250 feet per second (76 m/sec).

The data are shown as points, and the dashed lines indicate values of l_{eff} predicted by empirical correlations shown in equations (30) to (34).

The expression for l_{eff} without mean flow past or through the aperture is

$$l_{\text{eff}} = l + \delta \quad (30)$$

where

$$\delta = 0.85 d \left(1 - 0.7 \sqrt{\frac{A}{\text{cavity area}}} \right) \quad (\text{ref. 1}) \quad (31)$$

The topmost dashed line in figure 10 is based on equation (30).

The expression generally used to calculate the saturated or minimum l_{eff} is taken from figure 9; it is as follows:

$$l_{\text{eff}}(\text{saturated}) = 0.375 (l + \delta) \quad (32)$$

The bottom dashed line in figure 10 represents this expression.

Based on a limited quantity of data, the results of reference 8 indicate that the following expression may be valid:

$$l_{\text{eff}}(\text{saturated}) = l \quad (33)$$

The line representing equation (33) is indicated as such in figure 10.

Of these three correlations, equation (33) seems to represent the data best; however, it is still not satisfactory.

Equation (32) was developed from experiments using small aperture thicknesses ($l = 0.010$ to 0.118 in. or 0.05 to 0.3 cm) so that the aperture effective length correction factor δ was significantly larger than the thickness l . Therefore, the data cannot distinguish whether flow reduces $l + \delta$ or only δ . Reference 10 presents a theoretical argument showing that, for thin orifices ($l \approx 0$), the aperture effective length is reduced by turbulence to 0.375 times its original value. Consequently, a proposed expression for the saturated l_{eff} for thick-wall resonators is

$$l_{\text{eff}}(\text{saturated}) = l + 0.375 \delta \quad (34)$$

The dashed line, representing equation (34) and indicated as such in figure 10, agrees best with the data, indicating that equation (34) should be valid for the high mean flows associated with rocket engine liners.

Discussion of Nonlinear Resonator Model

As indicated in the INTRODUCTION, an important step in the calculation of θ , the acoustic resistance, is the formulation and validation of a nonlinear resonator model. The model is formulated and presented in the section Nonlinear Resonator Model. A typical result of using the model is shown in figure 11. The output presented in the calculated cavity pressure as a function of normalized time. The input parameters are $P'_{1, \text{max}} = 0.10$, $r = 0$, $\gamma = 1.2$, $\beta = 0.10$, and $\bar{\alpha}^2 = 1.00$. These values were chosen to correspond to those presented in reference 7. The results reach a steady state after the first cycle at a peak-to-peak value of 0.365 chamber pressure with a direct-current shift

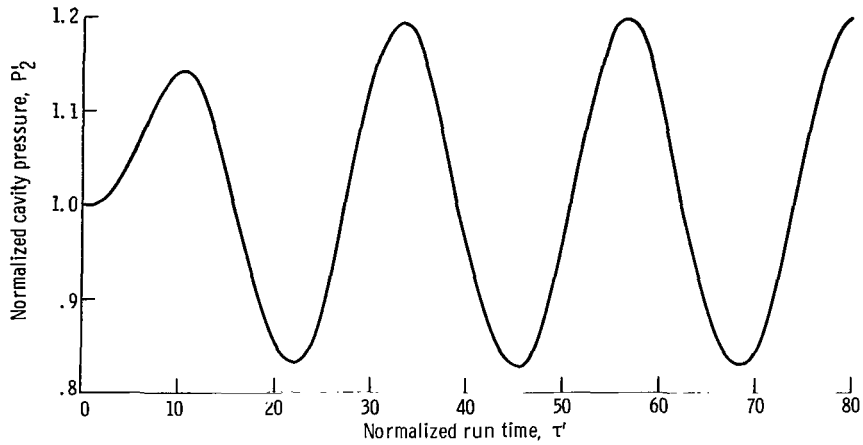


Figure 11. - Output of nonlinear model cavity pressure response. Ratio of frequency to Helmholtz frequency $f/f_{\text{Helmholtz}} = 0.855$; ratio of heat capacities $\gamma = 1.2$; $\bar{\alpha}^2 = 1.0$; dimensionless cavity geometry $\beta = 0.1$; dimensionless weight flow $r = 0$; maximum chamber pressure $P'_{1, \text{max}} = 0.10$.

of 0.012 chamber pressure. This shift is due to the assumptions inherent in the model and the nonlinearity of the model.

Both the velocity and cavity pressure outputs as a function of normalized frequency are shown in figure 12. The value taken as representative of the output is one-half the peak-to-peak value. These representative values are indicated by $\Delta U'$ and $\Delta P'_2$. The normalized frequency is the ratio of wave frequency to Helmholtz resonator frequency ω/ω_0 . For purposes of comparison, the results of the same configuration as presented in reference 7 are superimposed. The good agreement indicates the comparability of the

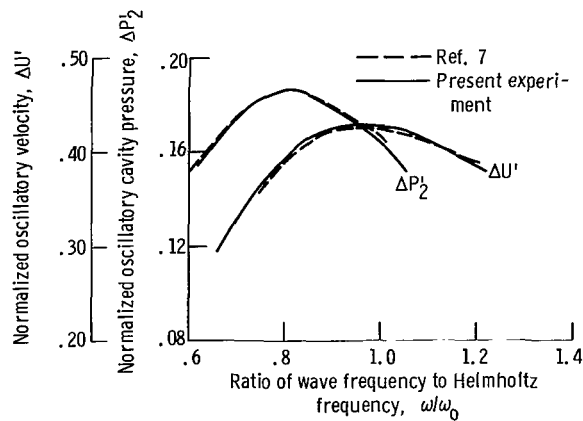


Figure 12. - Normalized oscillatory velocity and normalized oscillatory cavity pressure as function of ratio of wave frequency to Helmholtz frequency. $\bar{\alpha}^2 = 1.0$; dimensionless cavity geometry $\beta = 0.10$; dimensionless weight flow $r = 0$; maximum chamber pressure $P'_{1, \text{max}} = 0.10$.

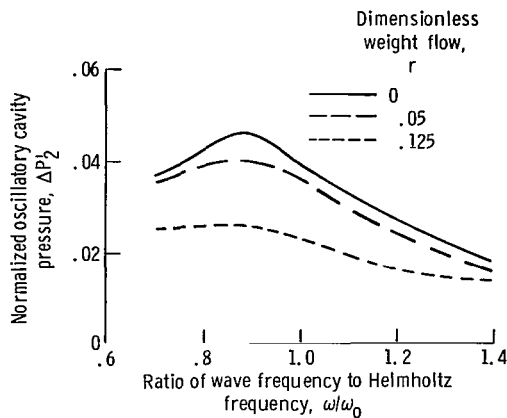


Figure 13. - Effect of mean flow through on resonator response as function of ratio of wave frequency to Helmholtz frequency. Ratio of heat capacities $\gamma = 1.6$; $\bar{\alpha}^2 = 1.0$; dimensionless cavity geometry $\beta = 0.02$; maximum chamber pressure $P_{1, \max}^1 = 0.02$.

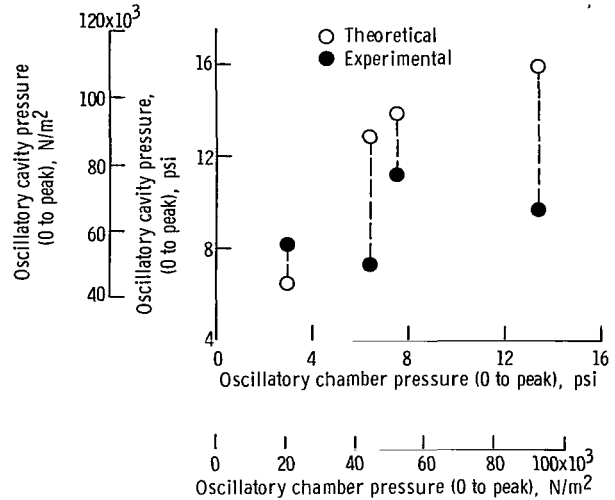


Figure 14. - Comparison of theoretical and experimental oscillatory cavity pressures as function of oscillatory chamber pressures for 90° phase lag. Frequency $f = 5300$ hertz.

integration procedures. The velocity maximizes in the region of ω/ω_0 , whereas the cavity pressure maximizes at frequency ratios of less than 1. The results are similar to the response of a forced-motion mass-spring-damper system with the shift in the peak cavity pressure response a function of the resonator damping.

The effect of purge flow on the oscillatory cavity pressure is presented in figure 13. The results are presented as a function of the dimensionless frequency ω/ω_0 for various values of dimensionless weight flow r defined as $(w/A)/\rho_0 c_0$. The values of γ , β , $\bar{\alpha}^2$, and $P_{1, \max}^1$ are representative of experimentally measured values. As r is increased, the cavity pressure response curve becomes lower and flatter in the same manner as would be expected for large increases in the aperture damping.

In order to validate the resonator model, the cavity gas composition, temperature, cavity depth, and oscillatory combustion pressures were converted to input parameters and the oscillatory cavity pressure calculated. Presented in figure 14 is a comparison of the corresponding theoretical and experimental oscillatory cavity pressures. Because of the difficulty in measuring the oscillatory pressures at a specific time in the run, a phase angle of 90° between combustor and cavity oscillatory pressures was used to define the only time at which theory and experiment were compared. The correspondence between theoretical and experimental values is indicated by the dashed lines in the figure.

Although the agreement was fairly good and tended to suggest the validity of the model, the lack of better agreement was likely because of the following factors:

- (1) There is no provision in the model for including the effects of mean flow past.

(2) Inherent in the model is the assumption that the γ within the cavity is the same as in the combustor. This assumption is in error by 30 percent, which can introduce changes in predicted values by up to 30 percent, but no change in trends.

(3) The validation of the model depends on correlating the temperatures, cavity depths, and oscillatory pressure amplitudes all at precisely the same time. This is particularly difficult with pressure oscillations that demonstrated variations over 30 percent during a short time period.

(4) The inability to measure the oscillatory combustor pressure immediately adjacent to the resonator aperture. The relation between the oscillatory pressure at the resonator aperture and the closest measurement point ($2\frac{1}{2}$ in. or 6.35 cm away) could not be precisely calculated and, therefore, the two were assumed equal.

Considering all of the possible sources of error, the agreement shown can be considered a limited verification of the model.

Calculation of Resistance θ

If it is assumed that the comparison between theory and experiment shown in figure 15 represents a limited verification of the resonator model, it is then reasonable to use the model to compute values of the resistance for various conditions with and without mean through flow.

The results of a number of variations in oscillatory chamber pressure and mean flow are presented in figure 15. The variations in oscillatory chamber pressure cause varia-

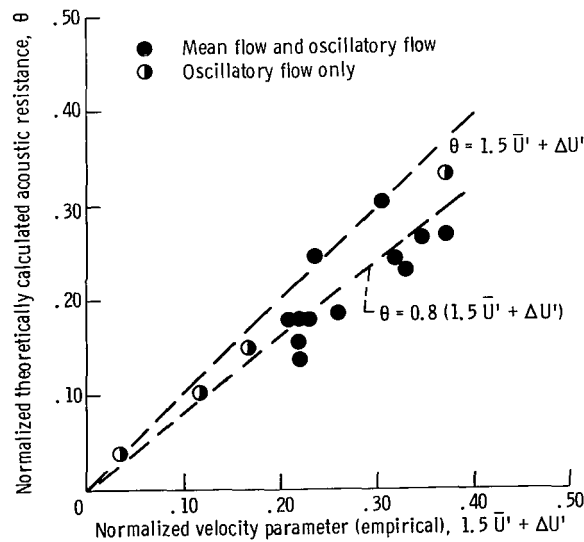


Figure 15. - Correlating theoretically calculated acoustic resistance with empirical normalized velocity parameter.

tions in oscillatory flow velocity. The acoustic resistance, defined in the section Theory as the ratio of normalized oscillatory chamber pressure to normalized in-phase aperture velocity, is plotted as a function of an empirical correlation of mean and oscillatory flows. The empirical correlation is arrived at as follows: the results of the study reported in reference 11 indicated that the nonnormalized acoustic resistance R can be expressed as

$$R = 1.5 \rho_0 \bar{U} \quad (35)$$

when \bar{U} is significantly larger than ΔU , the oscillatory velocity. When a pressure loss term of the form $\rho_0 U^2$ is assumed, in the absence of mean flow, R can be expressed as

$$R = \rho_0 \Delta U \quad (36)$$

An empirical combination of equations (35) and (36) is

$$\frac{R}{\rho_0} = 1.5 U + \Delta U \quad (37)$$

Normalizing equation (37) gives the following:

$$\theta = 1.5 \bar{U}' + \Delta U' \quad (38a)$$

Equation (38a) is presented as the upper dashed line in figure 15. The computed values lie somewhat lower as indicated by the symbols. The half-filled symbols, representing oscillatory flow only, seem to agree with the empirical dashed line better than the points representing both mean and oscillatory flows. As the flow velocities increase, the results deviate increasingly from the empirical correlation because the pressure loss term used in the model is not $\rho_0 \bar{U}^2$ but the more complicated expression of equation (9). The difference between these two pressure loss terms increases with increasing velocity. A more suitable expression for the resistance which better fits the results is

$$\theta = 0.8(1.5 \bar{U}' + \Delta \bar{U}') \quad (38b)$$

This expression is shown as the lower dashed line in figure 15. The use of the empirical model, as represented by equation (38b), would greatly simplify previous liner design calculations (e.g., ref. 1).

Use of the Empirical Resistance Equation

The use of the empirical resistance equation (eq. (38b)) can be demonstrated using α , the acoustic absorption coefficient. Under certain conditions, α can characterize the liner damping (ref. 12). In order to use α , the resistance of a single resonator θ must be converted into the resistance of an array of resonators Φ . This is accomplished by dividing θ by the liner open area ratio σ so that the following equation results:

$$\Phi = \frac{\theta}{\sigma} \quad (39)$$

The equation for α for a liner that is tuned is

$$\alpha = 4 \frac{\Phi}{(\Phi + 1)^2} \quad (40)$$

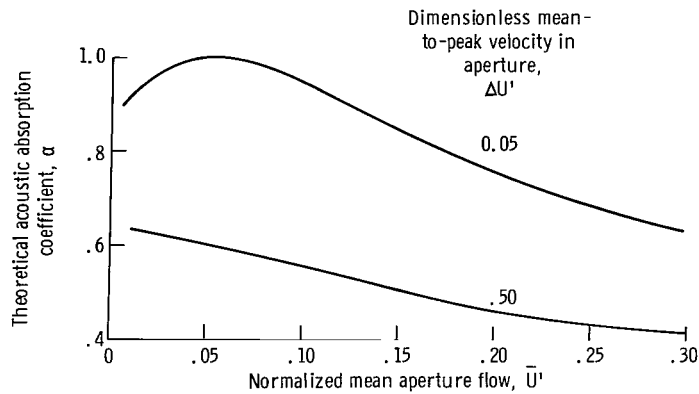


Figure 16. - Effect of mean flow on acoustic absorption coefficient α . Liner is tuned; open area ratio $\sigma = 0.10$; acoustic resistance of resonator $\theta = 0.8 (1.5 \bar{U}' + \Delta U')$.

Combining equations (38a), (39), and (40), the variation of α as a function of \bar{U}' for two values of $\Delta U'$ is calculated and presented in figure 16. The mean flow can decrease the absorption coefficient by a factor of two, although its effect is lessened for higher values of oscillatory flow $\Delta U'$. The results shown in figure 16 are important since they demonstrate that when a large value of gas purge flow is required to fix liner cavity properties, it can seriously reduce liner absorption.

SUMMARY OF RESULTS

Comparison of the calculated values of aperture effective length l_{eff} with empirical correlations indicate that the following expression should be used in a rocket engine liner with high mean flow past or through the aperture:

$$l_{\text{eff}} = l + 0.375 \delta$$
$$\delta = 0.85 d \left(1 - 0.7 \sqrt{\frac{A}{\text{cavity area}}} \right)$$

where l is aperture length, δ is aperture effective length correction, d is aperture diameter, and A is aperture area.

There is reasonable agreement between the theoretically calculated values of cavity oscillatory pressure and those which were experimentally measured. Using the theoretical model, values of the acoustic resistance, θ , were calculated. Comparison of the calculated values of θ with an empirical correlation indicated that the following expression best represented the data:

$$\theta = 0.8(1.5 \bar{U}' + \Delta U')$$

where \bar{U}' is nondimensional mean velocity in aperture and $\Delta U'$ is nondimensional mean-to-peak velocity in aperture.

Lewis Research Center,
National Aeronautics and Space Administration,
Cleveland, Ohio, December 12, 1968,
128-31-06-05-22.

REFERENCES

1. Wanhainen, John P.; Bloomer, Harry E.; Vincent, David W.; Curley, Jerome K.: Experimental Investigation of Acoustic Liners to Suppress Screech in Hydrogen-Oxygen Rockets. NASA TN D-3822, 1967.
2. Alexander, George: Acoustic Liner Damps Rocket Combustion Instability. Aviation Week & Space Technology, vol. 83, no. 6, Aug. 9, 1965, pp. 72, 73, 75, 77, and 79.

3. Ingard, Uno: On the Theory and Design of Acoustic Resonators. *J. Acoust. Soc. Am.*, vol. 25, no. 6, Nov. 1953, pp. 1037-1061.
4. Blackman, A. W.: Effect of Nonlinear Losses on the Design of Absorbers for Combustion Instabilities. *ARS J.*, vol. 30, no. 11, Nov. 1960, pp. 1022-1028.
5. Mechel, F.; Mertens, P.; and Shilz, W.: Research on Sound Propagation in Sound-Absorbant Ducts with Superimposed Air Streams. Final Rep., Göttingen Univ. (ARML-TDR-62-140, vol. II and III), Dec. 1962.
6. McAuliffe, Clinton E.: The Influence of High Speed Airflow on the Behavior of Acoustical Elements. M. Sc. Thesis, Mass. Inst. Tech., 1950.
7. Crocco, L., et al: Nonlinear Aspects of Combustion Instability on Liquid Propellant Rocket Motors. Rep. AMS-SR-553-g, Princeton Univ. (NASA CR-72270), June 1967.
8. Phillips, Bert: Effects of High-Wave Amplitude and Mean Flow on a Helmholtz Resonator. NASA TM X-1582, 1968.
9. Phillips, Bert: Experimental Investigation of an Acoustic Liner with Variable Cavity Depth. NASA TN D-4492, 1968.
10. Westervelt, P. J.: Acoustical Impedence in Terms of Energy Functions. *J. Acoust. Soc. Am.*, vol. 23, no. 3, May 1951, pp. 347-348.
11. Ingard, Uno; and Ising, Hartmut: Acoustic Nonlinearity of an Orifice. *J. Acoust. Soc. Am.*, vol. 42, no. 1, July 1967, pp. 6-17.
12. Phillips, Bert: On the Design of Acoustic Liners for Rocket Engines: Maximum Damping as a Design Objective. NASA TM X-1720, 1969.

FIRST CLASS MAIL

69030 00903
RECEIVED 54 JUL 30 1964
RESEARCH LABORATORY/AFSL/
TRIAL AIR FORCE BASE, MEXICO 9711

RECEIVED 54 JUL 30 1964

POSTMASTER: If Undeliverable (Section 158
Postal Manual) Do Not Return

"The aeronautical and space activities of the United States shall be conducted so as to contribute . . . to the expansion of human knowledge of phenomena in the atmosphere and space. The Administration shall provide for the widest practicable and appropriate dissemination of information concerning its activities and the results thereof."

— NATIONAL AERONAUTICS AND SPACE ACT OF 1958

NASA SCIENTIFIC AND TECHNICAL PUBLICATIONS

TECHNICAL REPORTS: Scientific and technical information considered important, complete, and a lasting contribution to existing knowledge.

TECHNICAL NOTES: Information less broad in scope but nevertheless of importance as a contribution to existing knowledge.

TECHNICAL MEMORANDUMS: Information receiving limited distribution because of preliminary data, security classification, or other reasons.

CONTRACTOR REPORTS: Scientific and technical information generated under a NASA contract or grant and considered an important contribution to existing knowledge.

TECHNICAL TRANSLATIONS: Information published in a foreign language considered to merit NASA distribution in English.

SPECIAL PUBLICATIONS: Information derived from or of value to NASA activities. Publications include conference proceedings, monographs, data compilations, handbooks, sourcebooks, and special bibliographies.

TECHNOLOGY UTILIZATION PUBLICATIONS: Information on technology used by NASA that may be of particular interest in commercial and other non-aerospace applications. Publications include Tech Briefs, Technology Utilization Reports and Notes, and Technology Surveys.

Details on the availability of these publications may be obtained from:

SCIENTIFIC AND TECHNICAL INFORMATION DIVISION
NATIONAL AERONAUTICS AND SPACE ADMINISTRATION
Washington, D.C. 20546